Colloid Polym Sci (2016) 294:1369–1379
DOI 10.1007/s00396-016-3893-8

ORIGINAL CONTRIBUTION

Sorption of Pb(II) on carboxymethyl chitosan-conjugated magnetite nanoparticles: application of sorbent dosage-dependent isotherms

Song Lu[1] · Haiping Li[2] · Fengrong Zhang[1] · Na Du[3] · Wanguo Hou[3]

Received: 20 January 2016 / Revised: 10 March 2016 / Accepted: 30 May 2016 / Published online: 8 June 2016

Abstract Carboxymethyl chitosan (CMCS)-conjugated magnetite (Fe_3O_4) nanoparticles (MNPs), which are denoted as CMCS-MNPs, were synthesized by covalently binding CMCS onto the surface of the MNPs via carbodiimide activation in a paraffin-acetic acid medium. The CMCS-MNPs exhibited a high level of CMCS binding (~24.7 wt.%) and a spherical morphology with a mean diameter of 15 nm. In particular, they showed good water dispersity and a strong magnetic response. The sorption of Pb(II) on the CMCS-MNPs in aqueous solutions at different sorbent dosages (C_s), pH, electrolyte ($NaNO_3$) concentrations (C_{NaNO3}), and temperatures (T) was investigated. The CMCS-MNPs showed high sorption capacity for Pb(II). The equilibrium amount increased with increasing pH but decreased with increasing C_{NaNO3} or T. In addition, a significant C_s-effect was observed in the sorption equilibria. Two C_s-dependent models, the Langmuir-SCA and Freundlich-SCA isotherms that were derived from a surface component activity (SCA) model, could describe the C_s-effect observed. The changes in pH, C_{NaNO3}, and T have no obvious influence on the C_s-effect. In addition, the changes in the thermodynamic parameters, $\Delta G°$, $\Delta H°$, and $\Delta S°$, for sorption were estimated, showing that the sorption process is spontaneous and exothermic.

Keywords Sorption · Sorbent effect · Carboxymethyl chitosan · Magnetic nanoparticle · Pb(II) · Surface component activity model

Research highlights:
1. Carboxymethyl chitosan-conjugated Fe_3O_4 nanoparticles, CMCS-MNPs, were synthesized.
2. CMCS-MNPs are an effective sorbent for the removal of Pb(II) from solution.
3. A sorbent effect (C_s-effect) was observed for Pb(II) sorption on the CMCS-MNPs.
4. The C_s-effect could be described using the Langmuir-SCA and Freundlich-SCA models.
5. The pH, electrolyte, and temperature had no obvious influence on the C_s-effect.
6. Pb(II) sorption on the CMCS-MNPs is spontaneous and exothermic in nature.

Electronic supplementary material The online version of this article (doi:10.1007/s00396-016-3893-8) contains supplementary material, which is available to authorized users.

✉ Wanguo Hou
wghou@sdu.edu.cn

[1] Environment Research Institute, Shandong University, Jinan 250100, People's Republic of China

[2] National Engineering Research Center for Colloidal Materials, Shandong University, Jinan 250100, People's Republic of China

[3] Key Laboratory of Colloid and Interface Chemistry (Ministry of Education), Shandong University, Jinan 250100, People's Republic of China

Introduction

Heavy metal pollution in aquatic systems is a serious environmental problem because of their high toxicity and non-biodegradability [1–4]. For example, Pb(II) is a common heavy metal pollutant resulting from both natural and anthropogenic sources. Long-term consumption of Pb(II) may cause serious health disorders, such as anemia, cancer, kidney disease, and mental retardation [5, 6]. According to the World Health Organization (WHO), the concentration of Pb(II) in drinking water should be lower than 10 μg/L [7]. Therefore, the removal of heavy metal pollutants has become a hot topic in environmental science and technology. Sorption is the primary technology considered for wastewater treatments because of its simplicity, low cost, high efficiency, and wider adaptability compared with alternative techniques, such as

extraction, precipitation, ion exchange, membrane filtration, and chemical oxidation [2–4]. From both theoretical and practical aspects, it is essential to understand the thermodynamic behavior of a sorption process. The Langmuir and Freundlich isotherms are the most widely used thermodynamic models to describe sorption isotherms. Because both classical isotherms are thermodynamic equilibrium equations [8], their model parameters should be independent of both the sorbate and sorbent concentrations for a given system under a constant temperature, pressure, and medium composition (e.g., pH and ionic strength) [9]. However, several studies [10–19] have reported that the parameters of the two classical models simulated using experimental data vary with the sorbent dose (C_s). This phenomenon is known as the sorbent effect (C_s-effect) [10]. In nature, sorbent particle–particle interactions exist in real sorption systems but the Langmuir and Freundlich models do not account for these interactions. They can describe the sorption behaviors of ideal systems, in which there are no interactions among solid particles, but cannot predict the C_s-effect observed in real systems. In fact, the parameter, C_s, is not present in the two model equations. The uncertainty in the model parameters at various C_s values limits the applicability of the two classical thermodynamic models because the model parameter values obtained at given C_s values cannot be used to make an accurate prediction of the sorption behavior at other C_s values.

Many models have been developed to describe the apparent C_s dependence of the sorption equilibria, including the particle interaction model [12], metastable equilibrium sorption theory [9], flocculation model [13], and power function (Freundlich-like) model [14]. Recently, we developed a surface component activity (SCA) model [20–22] in which the activity coefficient of the solid surface component sorption sites was assumed to be a function of C_s rather than unity because of the deviations in the behavior of a real sorption system from that of an ideal one. The C_s-dependent Langmuir and Freundlich isotherms, which are denoted as the Langmuir-SCA and Freundlich-SCA isotherms for clarity, were derived using the SCA model [21, 22]. The parameters of the two SCA model equations are C_s independent. Our previous work showed that the SCA model could describe C_s-dependent sorption in some systems [16–19]. However, there remains an urgent need to further examine the general applicability of the SCA model in describing the sorption equilibria with the C_s-effect. In particular, the effects of environmental factors, such as pH, ionic strength, and temperature, on the activity coefficient of solid sorption sites are unclear and require further investigation.

In this study, carboxymethyl chitosan (CMCS)-conjugated magnetite (Fe_3O_4) nanoparticles (MNPs) [23, 24], denoted as CMCS-MNPs, were synthesized and the sorption of Pb(II) on these CMCS-MNPs in aqueous solutions was examined at various C_s values. Special emphasis was placed on the applicability of the SCA model in describing the sorption equilibria, particularly the effects of pH, electrolyte ($NaNO_3$) concentration, and temperature on the activity coefficient of the solid sorption sites.

Recently, chitosan (CS), an *N*-deacetylated derivative of chitin, has attracted considerable attention as a promising sorbent because it is efficient, inexpensive, biodegradable, nontoxic, and environmentally friendly [2–4, 23–28]. CS molecules contain a substantial number of reactive hydroxyl (−OH) and amino ($-NH_2$) groups that can bind to toxic pollutants such as Pb(II), Cu(II), Hg(II), Cr(VI), Congo red, methylene blue, and tartrazine. However, the disadvantage of this sorbent is its weak acid resistance (i.e., quite soluble in acidic solutions) [26, 27]. To enhance its stability under acidic conditions, cross-linking and solid particle coupling treatments for CS are commonly employed [2, 3, 27, 29, 30]. One promising approach is to first carboxylate the CS molecules using, for example, chloroacetic acid [23, 24, 26–28] and alpha-ketoglutaric acid [25] and then bind it covalently onto the MNP surface through chemical reaction between the carboxyl groups of carboxylated CS and the hydroxyl groups of MNPs, forming magnetic CS nanoparticles [4]. The carboxyl groups of carboxylated CS can also supply additional sorption sites that may enhance the sorption capability of the CS. The conjugation of MNPs with CS can endow the CS sorbents with a magnetic response, resulting in their easy separation from aqueous solutions under an external magnetic field [4]. Magnetite is an ideal magnetic material because of its low cytotoxicity and good biocompatibility. Furthermore, the CS molecules bound in the magnetic CS sorbents might spread over the surface of MNPs, leading to the availability of almost all sorption sites [23], which is favorable for their applications in wastewater treatments. However, since Chang and Chen reported the CMCS-MNP sorbent in 2005 [23], only a few studies [24, 26–28] have focused on its sorption of heavy metals from aqueous solutions. Therefore, the present work improves the understanding of the thermodynamic behavior of sorption phenomena with C_s-effect and can help to evaluate the potential of CMCS-MNPs as sorbents for the removal of heavy metals from wastewater.

Materials and methods

Materials

Chitosan with a deacetylation level of 80–90 %, $FeCl_3 \cdot 6H_2O$, $FeSO_4 \cdot 7H_2O$, $NaNO_3$, $Pb(NO_3)_2$, and chloroacetic acid were of analytical grade and purchased from Sinopharm Chemical Reagent Co., Ltd., China. Carbodiimide (cyanamide, 95 %) was obtained from Sun Chemical Technology (Shanghai) Co., Ltd., China. All the reagents were used without further

purification. The water was purified using a Hitech-Kflow water purification system (Hitech, China).

Preparation of CMCS-MNPs

Preparation of MNPs The MNPs were prepared using a co-precipitation method [31]. $FeCl_3 \cdot 6H_2O$ (5.406 g, 0.02 mol) and $FeSO_4 \cdot 7H_2O$ (2.780 g, 0.01 mol) were dissolved in 100 mL of water under flowing N_2. Under vigorous stirring, 30 mL of an NH_4OH solution (~25 %) was added to the solution to achieve chemical precipitation. During the reaction process, the pH was maintained at approximately 10. The mixture was heated at 80 °C for 4 h and then cooled naturally to room temperature. The resulting MNPs were collected using a magnet, washed thoroughly with ethanol and water, and finally dried in a vacuum oven at 60 °C.

Preparation of CMCS Chitosan was carboxymethylated using chloroacetic acid according to the method reported elsewhere [23, 32]. Chitosan (3.0 g) and NaOH (15.0 g) were added to 100 mL of isopropanol/water solution (volume ratio, 80/20), and the mixture was then incubated at 60 °C for 1 h to allow swelling and alkalization. Subsequently, 20 mL of chloroacetic acid–isopropanol solution (0.75 g/mL) was added dropwise to the mixture in 30 min, and the resulting mixture was allowed to react for 4 h at 60 °C. The reaction was quenched by adding 200 mL of ethanol/water solution (volume ratio, 70/30). The resulting CMCS was separated by centrifugation, rinsed with 70 and 99 % ethanol for desalting and dehydration, respectively, and then dried in a vacuum oven at 60 °C.

Preparation of CMCS-MNPs The CMCS-MNPs were prepared via carbodiimide activation according to the method in literature [23, 25]. A paraffin-acetic acid mixture was used as the reaction medium to increase the amount of CMCS binding on the MNPs. The MNPs (2.0 g) were washed twice with absolute ethanol and dispersed ultrasonically in a solution containing 150 mL of paraffin and 2.5 mL of span-80, followed by the addition of a solution of CMCS (3.0 g) in 75 mL of acetic acid. After ultrasonication for 15 min, the suspension was transferred to a three-necked flask with a mechanical stirrer, followed by the addition of 10 mL of a carbodiimide solution (30 g/L in 0.003 M phosphate buffer, pH 6.0, 1 M NaCl). After reaction for 8 h at 60 °C, the resulting CMCS-MNPs were collected using a magnet, washed with water and ethanol, and dried in a vacuum oven at 50 °C.

Characterization

Fourier transform infrared (FT-IR) spectroscopy was performed using KBr pellets on an ALPHA-T FT-IR spectroscope (Bruker, Germany) over the range of 400–4000 cm^{-1}, with a resolution of 2 cm^{-1}. ^1H NMR spectrum of CMCS was recorded on a Bruker Advance 300 spectrometer (Germany) in D_2O. X-ray diffraction (XRD) was performed on a D/max-rA model diffractometer (Bruker., Germany) using Cu Kα radiation ($\lambda = 1.5418$ Å) at 40 kV and 40 mA over the 2θ range of 10–80°. The morphologies were observed by transmission electron microscopy (TEM, JEM-2100, JEOL, Japan). Thermogravimetric analysis (TGA, SDT-Q-600, TA Instruments Co., Germany) was performed from ambient temperature to 800 °C at 10 °C/min in air. The magnetization curves were obtained at ambient temperature by vibrating sample magnetometry (VSM, JDM-13, Jilin University, China) in a magnetic field range of 0–20,000 Oe.

Sorption experiments

The sorption experiments were performed using a batch technique at different C_s, pH, salt ($NaNO_3$) concentrations (C_{NaNO3}), and temperatures (T). Pb(II) solutions at various concentrations (0–900 mg/L) were prepared by dissolving $Pb(NO_3)_2$ in water containing specific amounts of $NaNO_3$ (C_{NaNO3}, 0.001–0.500 M). The pH of the solutions was adjusted to the desired values (3.0–6.0) using either 1 M HNO_3 or 1 M NaOH. Known masses (0.025–0.250 g) of the CMCS-MNPs were added to 25 mL of the Pb(II) solutions in polyethylene centrifuge tubes. The centrifuge tubes were shaken using a thermostatic water bath shaker (Jiangsu Medical Instrument Factory, China) for 24 h at a given T (25–55 °C). The sorption kinetic tests showed that a contact time of 24 h was sufficient to reach sorption equilibrium (Fig. S1 in the Electronic Supplementary Material, ESM). The sorption systems (suspensions) were then filtered through a 0.45-μm membrane, and the concentrations of Pb(II) remaining in the filtrates were determined at 283.3 nm using flame atomic absorption spectrometry (TAS-990, Beijing Purkinje General Instrument Co., Ltd., China). The sorption amounts of Pb(II) on the sorbent were calculated as follows:

$$\Gamma_e = (C_0 - C_e)/C_s \quad (1)$$

where Γ_e (mg/g) is the equilibrium sorption amount, C_0 (mg/L) and C_e (mg/L) are the initial and remaining (equilibrium) concentrations, respectively, and C_s (g/L) is the sorbent dosage.

Each test run was performed in triplicate, and the final values were the means of the three measurements. The relative error was less than 5 %.

Results and discussion

Characterization of the CMCS-MNPs

The CMCS-MNPs were characterized by FT-IR, XRD, TEM, TGA, and VSM techniques. Figure 1a presents the FT-IR spectra of CS, CMCS, MNPs, and CMCS-MNPs. The strong

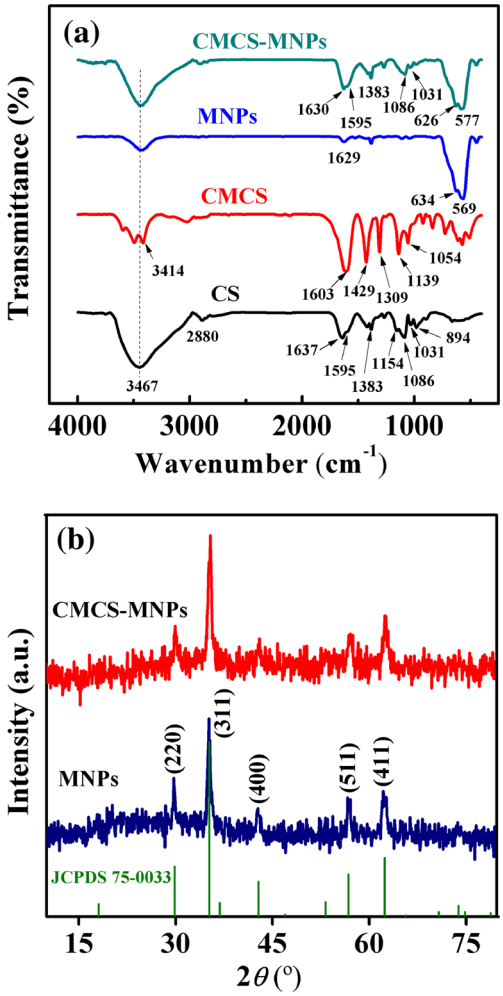

Fig. 1 (**a**) Fourier transform infrared (FT-IR) spectra of chitosan (CS), carboxymethyl chitosan (CMCS), magnetite (Fe_3O_4) nanoparticles (MNPs), and CMCS-MNPs. (**b**) X-ray diffraction (XRD) patterns of MNPs and CMCS-MNPs

and broad bands centered ~3467 cm^{-1} for various samples were assigned to the stretching vibration of the hydroxyl groups and adsorbed water molecules. The spectrum of CS revealed the following peaks: the band at ~2880 cm^{-1} was assigned to the C–H stretching vibration of the polymer backbone; the band at 1637 cm^{-1} was ascribed to the C=O stretching vibration in the amide groups; the band at 1595 cm^{-1} was attributed to the N–H bending vibration in the primary amine groups; the band at 1154 cm^{-1} was assigned to the C–O–C stretching vibration in the O-bridges; the bands at 1383 and 1031 cm^{-1} were attributed to the C–O stretching vibrations of the primary alcohol hydroxyl groups (–CH_2–OH on sixth carbon); the band at 1086 cm^{-1} was attributed to the C–O stretching vibration of secondary alcohol hydroxyl groups (–CH–OH on the rings); and the band at 894 cm^{-1} was assigned to the ring stretching vibration [25, 27, 32–34]. In the spectrum of CMCS, the band at 3414 cm^{-1} was attributed to the N–H bending mode in the primary amine groups [28], and the bands at 1603 and 1429 cm^{-1} were assigned to the asymmetric and symmetric stretching vibration of carboxyl group (COO^-), respectively. The adsorption at ~1603 cm^{-1} also contains the adsorptions arising from the C=O stretching vibrations of amide groups and the N–H bending of the primary amine groups [25, 34]. The bands at 1309, 1139, and 1054 cm^{-1} were assigned to the C–N stretching [33], C–O–C stretching, and C–OH stretching modes, respectively. In particular, the band strength at 1383 cm^{-1} corresponding to the CH_2–OH stretching band observed for CS was weakened in the spectrum of CMCS. This suggests that the carboxymethyl groups are linked to the hydroxyl groups of CS, which was also confirmed by NMR (Fig. S2 in the ESM). In the spectrum of bare MNPs, the band at 1629 cm^{-1} was attributed to the O–H vibration, indicating that the MNP surface is covered with hydroxyl groups, and the bands at 634 and 569 cm^{-1} were assigned to the Fe–O lattice vibrations [25]. For the CMCS-MNPs, the characteristic bands of CMCS and MNPs were observed in its spectrum. In particular, in the spectrum of CMCS-MNPs, the band at 1603 cm^{-1}, corresponding to the COO^- asymmetric stretching vibration of CMCS, was shifted to 1630 cm^{-1}, and the bands at 634 and 569 cm^{-1} corresponding to the Fe–O lattice vibrations of the MNPs were shifted to 626 and 577 cm^{-1}, respectively. These results suggest that CMCS is bound chemically to the Fe_3O_4 nanoparticles in CMCS-MNPs.

Figure 1b shows the XRD patterns of the MNPs and CMCS-MNPs. The MNPs exhibited the characteristic XRD peaks for the (220), (311), (400), (511), and (411) planes of Fe_3O_4 with a cubic spinel structure (JCPDS No. 75–0033). The XRD positions for CMCS-MNPs were similar. Figure 2 presents the TEM images of the MNPs and CMCS-MNPs. Both samples have similar morphologies, i.e., approximately monodisperse spherical particles with a mean diameter of 15 nm. XRD and TEM showed that the binding of CMCS has no obvious effect on the crystal structure and morphology of MNPs. This is similar to previous reports [23, 28].

Figure 3a shows the TGA curves of the MNPs, CMCS, and CMCS-MNPs. A weight loss at <120 °C was observed for all samples, which was assigned to the desorption of the physically adsorbed water. The amounts of physically adsorbed water for the MNPs, CMCS, and CMCS-MNPs were ~1.0, 3.5, and 9.0 wt.%, respectively. The MNPs show a weight loss of ~3.1 wt.% over the *T* range of 120–800 °C, which was attributed to the decomposition of surface hydroxyl groups. CMCS began to degrade at ~220 °C, and its weight loss at 120–800 °C was ~84.1 wt.%. The CMCS-MNPs exhibited a similar degradation temperature to that of the CMCS but a weight loss of only ~22.6 wt.% at 120–800 °C. Based on the TGA data, the amount of CMCS binding on the MNPs was estimated to be ~24.7 wt.%, which is higher than that (~5 wt.%) of the CMCS-MNPs synthesized in buffer solution (0.003 M phosphate, pH 6, 0.1 M NaCl) [23]. The

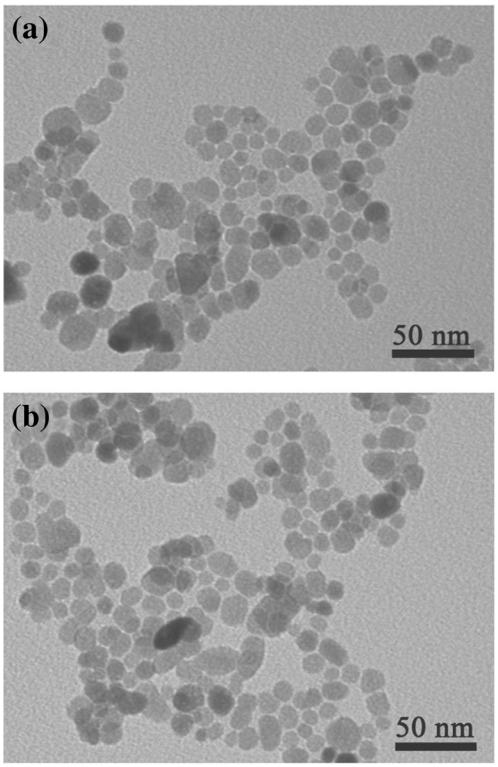

Fig. 2 Transmission electron microscopic (TEM) images of (**a**) MNPs and (**b**) CMCS-MNPs

magnetization curves of the MNPs and CMCS-MNPs (Fig. 3b) indicated that both samples were superparamagnetic with specific saturation magnetizations (M_s) of ~72 and 62 emu/g, respectively. The lower M_s value of the CMCS-MNPs compared to the MNPs is due to the presence of the nonmagnetic CMCS in the CMCS-MNPs. However, such CMCS-MNPs showed a strong response to an external magnetic field, as indicated by the following magnetic separation test. The CMCS-MNPs were dispersed in water in a glass vial by hand shaking, producing stable black homodispersion. This suggests that the CMCS-MNPs show good water dispersity. The black particles were attracted quickly to a magnet placed near the glass vial and the system became colorless and transparent within ~30 s (see the inset in Fig. 3b), demonstrating the strong magnetic sensitivity of the CMCS-MNPs. Therefore, the CMCS-MNPs can be separated easily by magnet after adsorbing pollutants from aqueous solutions.

Sorption isotherms

Figure 4a shows the sorption isotherms of Pb(II) on the CMCS-MNPs at four C_s values (1.00, 3.00, 5.00, and 10.0 g/L), where $T = 25 \pm 0.5$ °C, pH = 4.0, and $C_{NaNO3} = 0.010$ M. $NaNO_3$ was added to maintain a constant ionic strength. All the isotherms were L-type, and they significantly declined with increasing C_s.

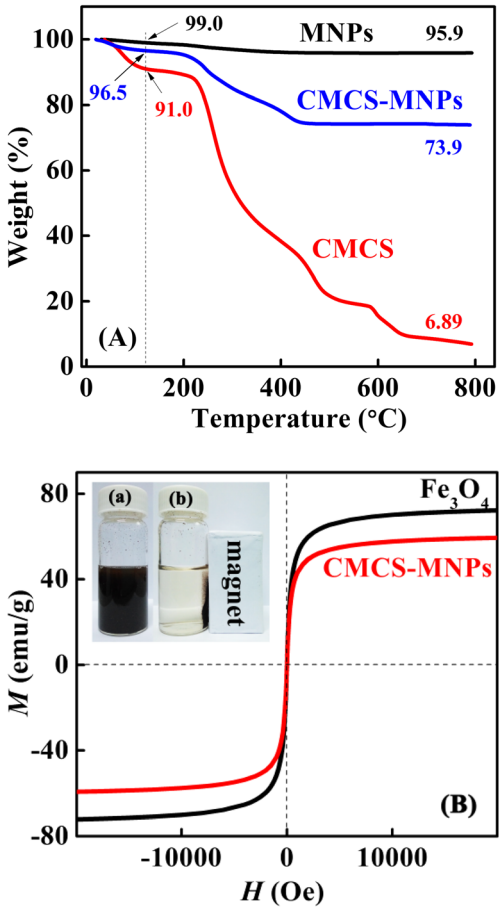

Fig. 3 (**A**) Thermogravimetric analysis (TGA) curves of MNPs, CMCS, and CMCS-MNPs. (**B**) Magnetization curves of MNPs and CMCS-MNPs. The inset in (**B**) shows a photograph of a CMCS-MNP dispersion (*a*) before and (*b*) after magnetic separation using a hand magnet

As we know, the L-type isotherms can be commonly described using the Langmuir and Freundlich models. The Langmuir and Freundlich isotherms can be expressed, respectively, as

$$\Gamma_e = \frac{K_L \Gamma_m C_e}{1 + K_L C_e} \tag{2}$$

$$\Gamma_e = K_F C_e^{n_F} \tag{3}$$

or in linear forms as

$$\frac{C_e}{\Gamma_e} = \frac{C_e}{\Gamma_m} + \frac{1}{K_L \Gamma_m} \tag{4}$$

$$\lg \Gamma_e = \lg K_F + n_F \lg C_e \tag{5}$$

where Γ_m (mg/g) is the monolayer saturated sorption amount, K_L (L/mg) is the Langmuir equilibrium constant, and K_F ($L^{n_F} \cdot mg^{1-n_F}/g$) and n_F are the Freundlich constants.

The sorption data at various C_s values were fitted to the Langmuir and Freundlich isotherms using nonlinear and linear regression methods, respectively, as shown in Fig. 4. The best-fit values of the model parameters, Γ_m, K_L, K_F, and n_F, as well

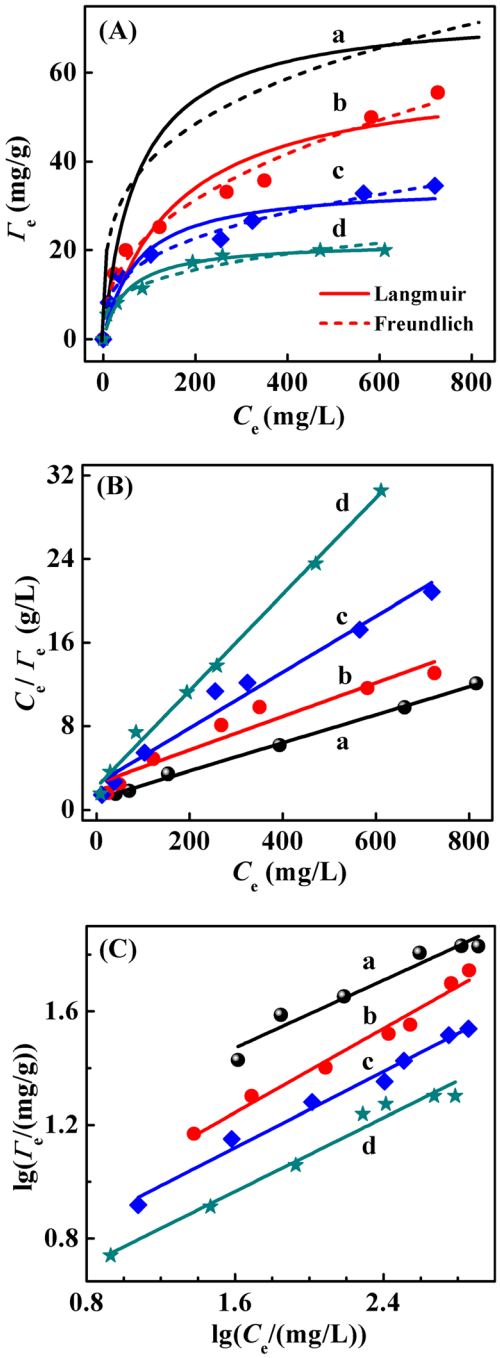

Fig. 4 (**A**) Sorption isotherms of Pb(II) on CMCS-MNPs at different C_s. The *dots* represent the experimental data; the *solid* and *dashed lines* represent the classical Langmuir and Freundlich fitting, respectively. Linear regression plots for classical (**B**) Langmuir and (**C**) Freundlich models. pH = 4.0, C_{NaNO3} = 0.010 M, T = 25 °C, and C_s values are (*a*) 1.00, (*b*) 3.00, (*c*) 5.00, and (*d*) 10.0 g/L

as the coefficient of determination (R^2), are listed in Table 1. The linear regression results in Fig. 4b, c show that both models can well describe the sorption isotherms for any given C_s value. However, the nonlinear regression results shown in Fig. 4a suggest that the Langmuir model is more suitable for these isotherms. In addition, all the model parameter values varied with C_s, and the Γ_m values decreased with increasing C_s, indicating that there is a C_s-effect in the sorption equilibria. As mentioned above, the Langmuir and Freundlich isotherms cannot describe or predict the C_s-effect observed in the sorption tests.

To examine the applicability of the SCA model in describing these sorption isotherms, the Langmuir-SCA and Freundlich-SCA isotherms were used to fit the sorption data. The Langmuir-SCA and Freundlich-SCA isotherms can be expressed, respectively, as [21, 22]

$$\frac{\Gamma_e}{f_s} = \frac{K_{eq}\Gamma_m^0 C_e}{1 + K_{eq}C_e} \tag{6}$$

$$\Gamma_e = K_S f_s C_e^{n_S} \tag{7}$$

or in linear forms as

$$\frac{f_s\Gamma_e}{C_e} = \frac{C_e}{\Gamma_m^0} + \frac{1}{K_{eq}\Gamma_m^0} \tag{8}$$

$$\lg\left(\frac{\Gamma_e}{f_s}\right) = n_S \lg C_e + \lg K_S \tag{9}$$

where f_s is the activity coefficient of the sorbent surface sites, K_{eq} is the intrinsic (or thermodynamic) equilibrium constant, Γ_m^0 is the characteristic saturation sorption capacity for a given system, corresponding to the saturated monolayer sorption of the total actual sorption sites, and K_S and n_S are the intrinsic Freundlich constants. The SCA model suggests that these intrinsic parameters, K_{eq}, Γ_m^0, K_S, and n_S, are independent of C_s for a given system under a constant temperature, pressure, and medium composition (e.g., pH and ionic strength) [21, 22]. If the Langmuir-SCA and Freundlich-SCA isotherms are applicable, the plots of f_sC_e/Γ_e vs. C_e and lg (Γ_e/f_s) vs. lg C_e should be linear and independent of C_s, and the plot of Γ_e/f_s vs. C_e for various C_s should be a unique curve.

In our previous work [17, 19–22], an exponential form of the C_s-dependent function of f_s was suggested as follows:

$$f_s = \exp\left(-\gamma C_s^{0.5}\right) \tag{10}$$

where γ is the empirical constant. The γ value can indicate the strength of the C_s-effect for a sorption system and a higher γ value represents a stronger C_s-effect. In addition, the relationships between the intrinsic parameters in the SCA model equations and the corresponding parameters in the classical Langmuir and Freundlich isotherms were obtained as follows [17, 19–22]:

$$\ln\Gamma_m = \ln\Gamma_m^0 - \gamma C_s^{0.5} \tag{11}$$

$$\ln K_F = \ln K_S - \gamma C_s^{0.5} \tag{12}$$

The two equations can be used to simulate the empirical constant, γ, in f_s from the sorption data.

Table 1 Isotherm parameters for Pb(II) sorption on CMCS-MNPs (pH = 4.0, C_{NaNO3} = 0.010 M, and T = 25 °C)

C_s (g/L)	Langmuir isotherm			Freundlich isotherm		
	Γ_m (mg/g)	K_L (L/mg)	R^2	K_F ($L^{n_F} \cdot mg^{1-n_F}/g$)	n_F	R^2
1.00	74.57	1.65×10^{-2}	0.997	9.829	0.2990	0.938
3.00	62.15	6.48×10^{-3}	0.919	4.482	0.3697	0.975
5.00	37.34	1.10×10^{-2}	0.968	3.837	0.3350	0.983
10.0	21.67	1.31×10^{-2}	0.995	2.795	0.2450	0.970

The plots of ln Γ_m vs. $C_s^{0.5}$ and ln K_F vs. $C_s^{0.5}$, which were obtained using the Γ_m and K_F data at various C_s values, showed reasonably straight lines (Fig. S3 in the ESM), indicating that Eqs. (11) and (12) are acceptable for the sorption systems studied. The γ value of Pb(II) sorption on the CMCS-MNPs obtained from the slopes of the two straight lines was 0.58 ± 0.02 $L^{0.5}/g^{0.5}$ (Table S1 in the ESM).

The sorption data at different C_s values were fitted to the Langmuir-SCA and Freundlich-SCA isotherms using the γ values, as shown in Fig. 5. As expected, the plots of Γ_e/f_s vs. C_e at various C_s values showed a unique C_s-independent curve, and those of both $f_s C_e/\Gamma_e$ vs. C_e and lg (Γ_e/f_s) vs. lg C_e were straight lines, which are consistent with the prediction of the SCA model. These results show that both the Langmuir-SCA and Freundlich-SCA models can adequately describe the sorption equilibria of Pb(II) on the CMCS-MNPs. The intrinsic model parameters, K_{eq}, Γ_m^0, K_S, and n_S, which were calculated from the slopes and intercepts of the linear model plots (Table S1 in the ESM), were 0.0121 L/mg, 146 mg/g, 14.6 $L^{n_s} \cdot mg^{1-n_s}/g$, and 0.330, respectively. These parameter values can be used to predict the Pb(II) sorption capacities of the sorbent at any C_s because of their C_s-independent features. As C_s can significantly influence the sorption capacity of sorbents, Γ_m^0 should be used instead of Γ_m at a given C_s to compare the sorption capacities of different sorbents.

Effects of pH, electrolyte, and temperature on sorption

The effects of environmental factors including pH, C_{NaNO3}, and T on Pb(II) sorption on the CMCS-MNPs were determined at various C_s values but with a constant C_0 of 500 mg/L. Figure 6a shows the pH dependence of Pb(II) sorption at C_{NaNO3} = 0.010 M and T = 25 °C. For any given C_s, the Γ_e increased with increasing pH from 3.0 to 6.0. Similar results have been reported [23, 26]. The driving force for Pb(II) sorption on CMCS-MNPs arises from the chelation between Pb(II) and the hydroxyl (–OH), amino (–NH_2), and carboxylate (–COO^-) functional groups of CMCS. At low pH, these functional groups

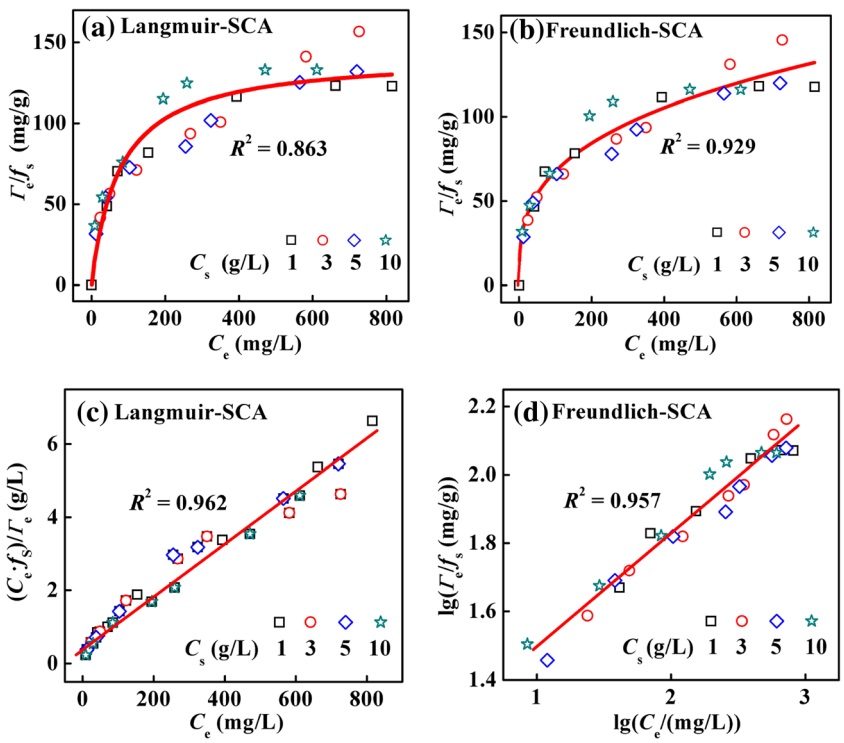

Fig. 5 (**a**, **b**) Nonlinear and (**c**, **d**) linear fitting plots of (**a**, **c**) Langmuir-SCA and (**b**, **d**) Freundlich-SCA models for Pb(II) sorption on CMCS-MNPs at pH = 4.0, C_{NaNO3} = 0.010 M, and T = 25 °C

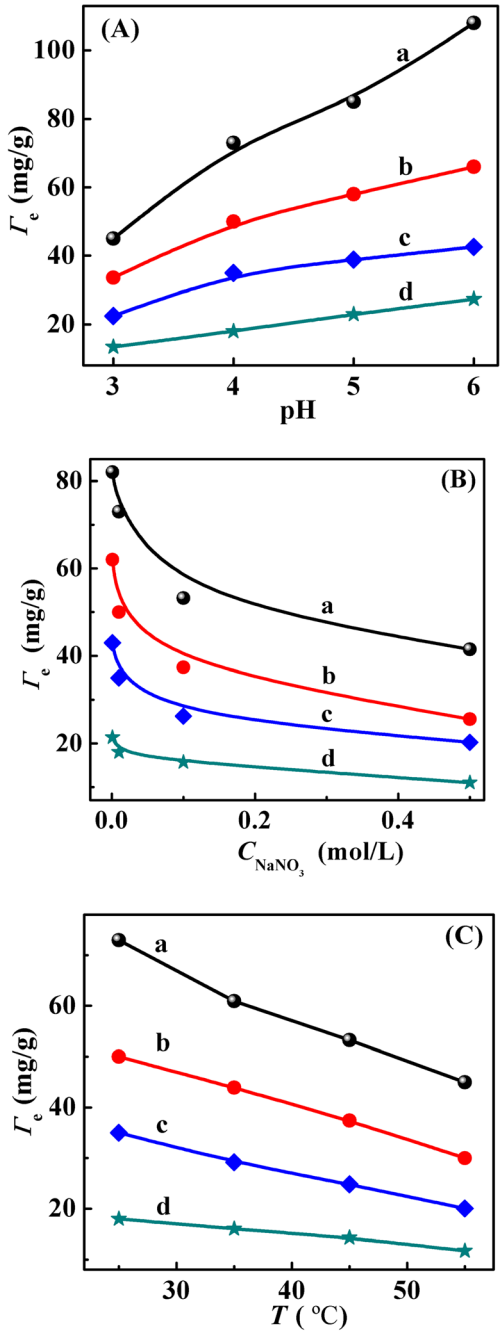

Fig. 6 Variations of Γ_e with (**A**) pH (C_{NaNO3} = 0.010 M, T = 25 °C), (**B**) C_{NaNO3} (pH = 4.0, T = 25 °C), and (**C**) T (C_{NaNO3} = 0.010 M, pH = 4.0) for Pb(II) sorption on CMCS-MNPs at different C_s. C_0 = 500 mg/L, and C_s values are (*a*) 1.00, (*b*) 3.00, (*c*) 5.00, and (*d*) 10.0 g/L

are protonated, resulting in weak chelation ability. With increasing pH, the functional groups of CMCS would gradually become deprotonated, which can strengthen the chelation ability and thus enhance the sorption. Notably, a white $Pb(OH)_2$ precipitate formed at pH >6, so no sorption tests were performed.

Figure 6b shows the C_{NaNO3} dependence of Pb(II) sorption at pH = 4.0 and T = 25 °C. At any given C_s, Γ_e decreased with increasing C_{NaNO3} from 0.001 to 0.500 M. This is because the presence of an electrolyte can restrain the chelation between Pb(II) and the functional groups of CMCS and can induce competitive sorption of its cations for the sorption sites. Figure 6c shows the T dependence of Pb(II) sorption at pH = 4.0 and C_{NaNO3} = 0.010 M. An increase in T from 25 to 55 °C causes a decrease in Γ_e at any given C_s, which is consistent with previous reports [23]. This is because a high temperature can weaken the chelation between Pb(II) and the functional groups of CMCS-MNPs.

Figure 6 also shows that Γ_e decreases with increasing C_s at any given pH, C_{NaNO3}, or T. This suggests that under the different conditions studied, the C_s-effect exists in the sorption equilibria. For a given C_0, there is a relationship between Γ_e and C_s as follows [17]:

$$\Gamma_e = \Gamma_e^0 \exp\left(-\gamma C_s^{0.5}\right) \tag{13}$$

or in a linear form as follows:

$$\ln \Gamma_e = \ln \Gamma_e^0 - \gamma C_s^{0.5} \tag{14}$$

where Γ_e^0 is the intrinsic sorption amount at a given C_0. This indicates that the empirical constant γ in f_s can be simulated from the sorption data at different C_s for a given C_0.

Each set of $\Gamma_e - C_s$ data for the given conditions was fitted to Eq. (14), and the results are shown in Fig. 7. All plots of ln Γ_e vs. $C_s^{0.5}$ showed reasonably straight lines, indicating that Eq. (14) is acceptable for sorption under the different conditions studied. The best-fit values of γ, Γ_e^0, and R^2 for the sorption data are listed in Table 2. No obvious change in the γ values (with a relative error less than 7 %) was observed under the conditions examined, indicating that a change in the environmental conditions does not obviously affect the C_s-effect strength of the sorption system. From the γ values obtained from the sorption equilibrium data at a single C_0, the mean γ value was calculated to be ~0.61 $L^{0.5}/g^{0.5}$, which is close to that obtained from the sorption isotherms (~0.58 $L^{0.5}/g^{0.5}$). In fact, although the C_s-effect arises from the sorbent particle–particle interactions in sorption systems, its strength is determined by the change in the strength of the particle–particle interactions with varying C_s. These results suggest that, under the conditions examined, a change in the environmental conditions has no effect on the C_s dependence of the strength of the particle–particle interactions, even though it can affect the strength of the particle–particle interactions.

Estimation of the changes in the thermodynamic parameters for sorption

The changes in thermodynamic parameters, including the Gibbs free energy ($\Delta G°$), enthalpy ($\Delta H°$), and entropy ($\Delta S°$), associated with a sorption process are commonly estimated from the partition coefficients ($K_p = \Gamma_e/C_e$), which are determined at different T for a given C_0 [23, 26, 28]. Owing to the C_s dependence of Γ_e and thus K_p (Fig. S4 in the ESM), the so-

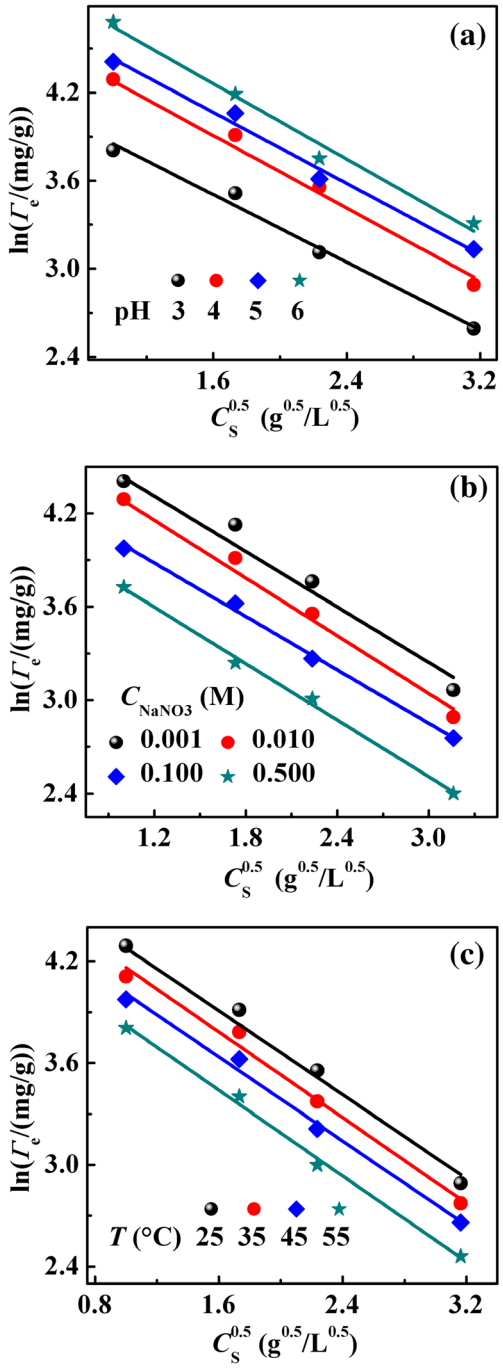

Fig. 7 Plots of ln Γ_e vs. $C_s^{0.5}$ for Pb(II) sorption on CMCS-MNPs at $C_0 = 500$ mg/L and different (**a**) pH ($C_{NaNO3} = 0.010$ M, $T = 25$ °C), (**b**) C_{NaNO3} (pH = 4.0, $T = 25$ °C), and (**c**) T ($C_{NaNO3} = 0.010$ M, pH = 4.0)

obtained values of the thermodynamic parameter changes would be C_s dependent. This is counter to the thermodynamic equilibrium law. Fundamentally, K_p obtained using the experimental Γ_e and C_e data is not a thermodynamic parameter and may be called an apparent partition coefficient. Therefore, we suggest that the changes in the thermodynamic parameters should be estimated from the intrinsic (or thermodynamic) partition coefficients (K_p^0) in the SCA model [20].

Table 2 SCA model parameters simulated using Eq. (14) for Pb(II) sorption on the CMCS-MNPs at $C_0 = 500$ mg/L and different pH, C_{NaNO3}, and T

pH	C_{NaNO3} (M)	T (°C)	Γ_e^0 (mg/g)	γ ($L^{0.5}/g^{0.5}$)	R^2
3.0	0.010	25.0	83.7	0.576	0.981
4.0	0.010	25.0	147	0.654	0.990
5.0	0.010	25.0	160	0.615	0.993
6.0	0.010	25.0	199	0.637	0.979
4.0	0.001	25.0	168	0.632	0.966
4.0	0.100	25.0	96.3	0.572	0.994
4.0	0.500	25.0	75.4	0.605	0.995
4.0	0.010	35.0	119	0.629	0.989
4.0	0.010	45.0	102	0.620	0.990
4.0	0.010	55.0	85.6	0.632	0.994

Based on the SCA model, a SCA-partition coefficient function was derived [20] and expressed as

$$K_p = \frac{\Gamma_e}{C_e} = f_s K_p^0 \tag{15}$$

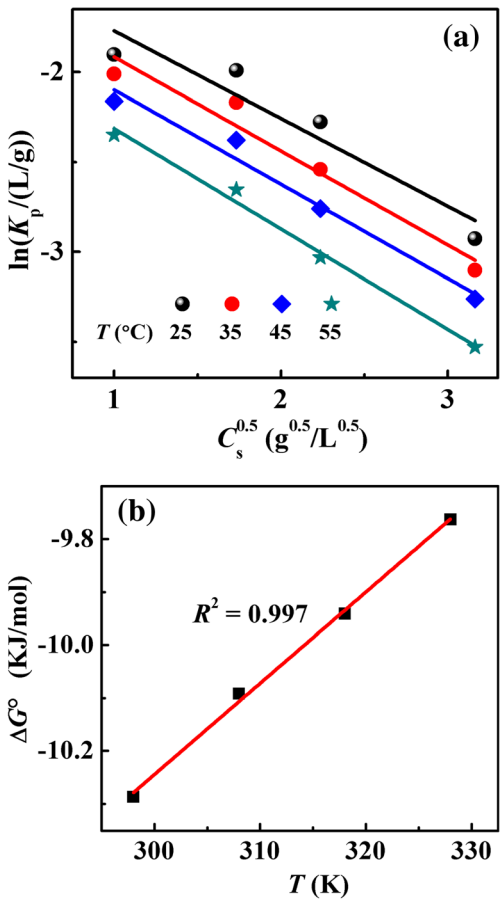

Fig. 8 Plots of (**a**) ln K_p vs. $C_s^{0.5}$ at different T and (**b**) $\Delta G°$ vs. T for Pb(II) sorption on CMCS-MNPs at $C_{NaNO3} = 0.010$ M and pH = 4.0

Table 3 Thermodynamic parameters of Pb(II) sorption on CMCS-MNPs at different T (C_{NaNO3} = 0.010 M, pH = 4.0)

T (K)	K_p^0 (L/mol)	R^2	$\Delta G°$ (kJ/mol)	ΔH (kJ/mol)	ΔS (kJ/mol K)
298	63.56	0.933	−10.29	−15.42	-1.72×10^{-2}
308	51.47	0.937	−10.09		
318	42.95	0.966	−9.937		
328	35.87	0.987	−9.761		

or in a linear form as

$$\ln K_p = -\gamma C_s^{0.5} + \ln K_p^0 \quad (16)$$

where K_p^0 is the intrinsic (or thermodynamic) partition coefficient that is C_s independent.

Each set of $K_p - C_s$ data at different T were fitted to Eq. (16), and the results are shown in Fig. 8a. All the plots of ln K_p vs. $C_s^{0.5}$ form reasonably straight lines. The best-fit values of K_p^0 and R^2 for the sorption data are listed in Table 3.

The thermodynamic parameter changes can be estimated from the K_p^0 values at different T using the following equations:

$$\Delta G^\circ = -RT \ln K_p^0 \quad (17)$$

$$\Delta G° = \Delta H° - T\,\Delta S° \quad (18)$$

where R is the gas constant (8.314 J/(mol K)), and T (in K) is the absolute temperature. The results are listed in Table 3. The negative $\Delta G°$ values indicate the spontaneous nature of Pb(II) sorption on the CMCS-MNPs, and the decrease in the absolute values of $\Delta G°$ with increasing T indicates that a high T is unfavorable for sorption. Plotting $\Delta G°$ vs. T resulted in a reasonable linear fit (Fig. 8b), and the $\Delta H°$ and $\Delta S°$ were estimated to be −15.42 kJ/mol and -1.72×10^{-2} kJ/(mol K) from the intercept and slope of the straight line, respectively. The negative $\Delta H°$ value indicates that the sorption process is exothermic in nature, which is consistent with previous reports [23, 26]. The negative $\Delta S°$ value suggests that the sorption process decreases the randomness of the system [24, 26, 27].

Conclusions

CMCS-MNPs containing ~24.7 wt.% CMCS were synthesized and assessed as a potential magnetic sorbent for removing the heavy metal Pb(II) from aqueous solutions. The level of Pb(II) sorption on the CMCS-MNPs increased with increasing pH (3.0–6.0) but decreased with increasing C_{NaNO3} (0.001–0.500 M) or T (25–55 °C). In addition, a significant C_s-effect was observed in the sorption of Pb(II) on the CMCS-MNPs. The classical Langmuir and Freundlich isotherms can well describe the sorption equilibria at each given C_s but cannot describe the C_s-effect observed. The C_s-effect data can be described using the Langmuir-SCA and Freundlich-SCA isotherms. Changes in environmental factors including pH, C_{NaNO3}, and T have no obvious influence on the C_s-effect. We suggest that the changes in the thermodynamic parameters of a sorption equilibrium process should be estimated from the intrinsic (or thermodynamic) partition coefficients rather than the apparent partition coefficients. Our results demonstrate that the sorption process is spontaneous and exothermic in nature. This study provides a better understanding of the C_s-effect phenomenon and confirms the applicability of the SCA model for describing the sorption equilibria with the C_s-effect.

Acknowledgments This work was financially supported by the National Natural Science Foundation of China (Nos. 21573133 and 21403128).

Compliance with ethical standards

Conflict of interest The authors declare that they have no conflict of interest.

References

1. Schwarzenbach RP, Escher BI, Fenner K, Hofstetter TB, Johnson CA, Von Gunten U, Wehrli B (2006) The challenge of micropollutants in aquatic systems. Science 313:1072–1077
2. Ngah WSW, Teong LC, Hanafiah M (2011) Adsorption of dyes and heavy metal ions by chitosan composites: a review. Carbohydr Polym 83:1446–1456
3. Reddy DHK, Lee S-M (2013) Application of magnetic chitosan composites for the removal of toxic metal and dyes from aqueous solutions. Adv Colloid Interface Sci 201:68–93
4. Nguyen TAH, Ngo HH, Guo WS, Zhang J, Liang S, Yue QY, Li Q, Nguyen TV (2013) Applicability of agricultural waste and by-products for adsorptive removal of heavy metals from wastewater. Bioresour Technol 148:574–585
5. Li Y-H, Wang S, Wei J, Zhang X, Xu C, Luan Z, Wu D, Wei B (2002) Lead adsorption on carbon nanotubes. Chem Phys Lett 357: 263–266
6. Zhao G, Ren X, Gao X, Tan X, Li J, Chen C, Huang Y, Wang X (2011) Removal of Pb (II) ions from aqueous solutions on few-layered graphene oxide nanosheets. Dalton Trans 40:10945–10952
7. Madadrang CJ, Kim HY, Gao G, Wang N, Zhu J, Feng H, Gorring M, Kasner ML, Hou S (2012) Adsorption behavior of EDTA-graphene oxide for Pb (II) removal. ACS Appl Mater Interfaces 4: 1186–1193
8. Sheindorf CH, Rebhun M, Sheintuch M (1981) A Freundlich-type multicomponent isotherm. J Colloid Interface Sci 79:136–142
9. Pan G, Liss PS (1998) Metastable-equilibrium adsorption theory: I. Theoretical. J Colloid Interface Sci 201:71–76
10. O'Connor DJ, Connolly JP (1980) The effect of concentration of adsorbing solids on the partition coefficient. Water Res 14:1517–1523
11. Voice TC, Weber WJ (1985) Sorbent concentration effects in liquid/solid partitioning. Environ Sci Technol 19:789–796
12. Di Toro DM, Mahony JD, Kirchgraber PR, O'Byrne AL, Pasquale LR, Piccirilli DC (1986) Effects of nonreversibility, particle concentration, and ionic strength on heavy-metal sorption. Environ Sci Technol 20:55–61

13. Helmy AK, Ferreiro EA, De Bussetti SG (2000) Effect of particle association on 2, 2′-bipyridyl adsorption onto kaolinite. J Colloid Interface Sci 225:398–402
14. Chang TW, Wang MK (2002) Assessment of sorbent/water ratio effect on adsorption using dimensional analysis and batch experiments. Chemosphere 48:419–426
15. Fehse K-U, Borg H, Sorkau E, Pilchowski K, Luckner L (2010) Correcting the effect of the sorbent to solution ratio on sorption isotherms from batch tests with soils and sediments. Water Air Soil Pollut 210:211–220
16. Guo Y, Hou W, Liang J, Liu J (2014) Sorbent concentration effect on adsorption of methyl orange on chitosan beads in aqueous solutions. Chem Res Chin Univ 30(5):837–843
17. Zhang F, Du N, Li H, Song S, Hou W (2015) Sorbent effect on the sorption of Cr (VI) on a Mg_6AlFe-layered double hydroxide and its calcined product in aqueous solutions. Colloid Polym Sci 293:1961–1969
18. Zhang F, Du N, Song S, Hou W (2015) Mechano-hydrothermal synthesis of SDS intercalated LDH nanohybrids and their removal efficiency for 2,4-dichlorophenoxyacetic acid from aqueous solution. Mater Chem Phys 152:95–103
19. Zhang F, Song Y, Song S, Zhang R, Hou W (2015) Synthesis of magnetite–graphene oxide-layered double hydroxide composites and applications for the removal of Pb (II) and 2, 4-dichlorophenoxyacetic acid from aqueous solutions. ACS Appl Mater Interfaces 7:7251–7263
20. Zhao L-X, Hou W-G (2012) The effect of sorbent concentration on the partition coefficient of pollutants between aqueous and particulate phases. Colloids Surf A Physicochem Eng Asp 396:29–34
21. Zhao L-X, Song S-E, Du N, Hou W-G (2013) A sorbent concentration-dependent Freundlich isotherm. Colloid Polym Sci 291:541–550
22. Zhao L-X, Song S-E, Du N, Hou W-G (2012) A sorbent concentration-dependent Langmuir isotherm. Acta Phys-Chim Sin 28:2905–2910
23. Chang Y-C, Chen D-H (2005) Preparation and adsorption properties of monodisperse chitosan-bound Fe_3O_4 magnetic nanoparticles for removal of Cu (II) ions. J Colloid Interface Sci 283:446–45
24. Chang YC, Chen DH (2005) Adsorption kinetics and thermodynamics of acid dyes on a carboxymethylated chitosan–conjugated magnetic nano–adsorbent. Macromol Biosci 5:254–261
25. Li G-y, Huang K-l, Jiang Y-r, Ding P, Yang D-l (2008) Preparation and characterization of carboxyl functionalization of chitosan derivative magnetic nanoparticles. Biochem Eng J 40:408–414
26. Kuang S-P, Wang Z-Z, Liu J, Wu Z-C (2013) Preparation of triethylene-tetramine grafted magnetic chitosan for adsorption of Pb (II) ion from aqueous solutions. J Hazard Mater 260:210–219
27. Mi F-L, Wu S-J, Chen Y-C (2015) Combination of carboxymethyl chitosan-coated magnetic nanoparticles and chitosan-citrate complex gel beads as a novel magnetic adsorbent. Carbohydr Polym 131:255–263
28. Nasirimoghaddam S, Zeinali S, Sabbaghi S (2015) Chitosan coated magnetic nanoparticles as nano-adsorbent for efficient removal of mercury contents from industrial aqueous and oily samples. J Ind Eng Chem 27:79–87
29. Muzzarelli RAA (2011) Potential of chitin/chitosan-bearing materials for uranium recovery: an interdisciplinary review. Carbohydr Polym 84:54–63
30. Hu X-j, Wang J-s, Liu Y-g, Li X, Zeng G-m, Bao Z-l, Zeng X-x, Chen A-w, Long F (2011) Adsorption of chromium (VI) by ethylenediamine-modified cross-linked magnetic chitosan resin: isotherms, kinetics and thermodynamics. J Hazard Mater 185:306–314
31. Liao M-H, Chen D-H (2002) Preparation and characterization of a novel magnetic nano-adsorbent. J Mater Chem 12:3654–3659
32. Chen X-G, Park H-J (2003) Chemical characteristics of O-carboxymethyl chitosans related to the preparation conditions. Carbohydr Polym 53:355–359
33. Yang J-H, Du Y-M, Qin C-Q (2003) Applications of infrared spectroscopy and nuclear magnetic resonance spectroscopy in the studies of the structure of chitin and chitosan. J Anal Sci 19:282–287
34. Guang G, Wu Z (2004) Structure and properties of carboxymethyl chitin. Polym Mater Sci Eng 20:107–110